RESERVE THIS SPACE

Molecular Dynamics Study of the Mechanism of Cellulose Dissolution in the Ionic Liquid 1-*n*-Butyl-3-Methylimidazolium Chloride

Zhiwei Liu,[1,2] Richard C. Remsing,[2] Preston B. Moore,[1,2] and Guillermo Moyna[1,2]

[1]West Center for Computational Chemistry and Drug Design and [2]Department of Chemistry & Biochemistry, University of the Sciences in Philadelphia, 600 South 43rd Street, PA 19104-4495

N,*N*'-Dialkylimidazolium ionic liquids (ILs) show promise as non-derivatizing 'green' solvents for the dissolution and processing of cellulose. To better understand how these ILs solvate this and other polysaccharides at the molecular level, we have performed molecular dynamics (MD) simulations of neat 1-*n*-butyl-3-methylimidazolium chloride ([C_4mim]Cl) at 298, 313, 333, 343, 353, 363, and 373 K, as well as 5 and 10 wt% cellobiose solutions in [C_4mim]Cl at 363 K. Static, dynamic, and thermodynamic quantities have been derived from the collected data. Our findings agree well with experimental data from various sources. In particular, analysis of structural features and hydrogen bonding patterns between [C_4mim]Cl and cellobiose are consistent with results from NMR relaxation studies which indicate that the IL Cl^- ions interact with the carbohydrate OH groups in a ~ 1:1 ratio.

RESERVE THIS SPACE

1. Introduction

In addition to their now well-established role as alternative reaction and extraction media with 'green' potential (*1*), it has been shown that certain ionic liquids (ILs) can dissolve polysaccharides very efficiently (*2-4*). Perhaps the most salient results in this regard have been those obtained with 1-*n*-butyl-3-methylimidazolium chloride ([C_4mim]Cl, Figure 1), an IL which dissolves cellulose in concentrations of up to 300 g/L (*2*). In a recent report, we studied the solvation of cellulose models, such as cellobiose (Figure 1), in [C_4mim]Cl by means of ^{13}C and $^{35/37}Cl$ NMR relaxation measurements (*5*). Our results indicate that the solvation of carbohydrates in this IL involves the formation of hydrogen bonds between the non-hydrated chloride ions of the IL and the sugar hydroxyl protons in a ~ 1:1 stoichiometry (*5*). In the case of cellulose, these interactions disrupt the extensive hydrogen bonding network of the polymer and lead to its dissolution. However, a detailed model of this dissolution mechanism is still unavailable. Knowledge of this process at the atomic level is critical in the development of new IL-based solvents for the processing of polysaccharides. As evidenced by the growing number of reports on the subject, many of which are referenced in this chapter or appear elsewhere in this volume, molecular dynamics (MD) simulations can provide this atomistic depiction of ILs and IL-based systems. In this chapter we describe the application of this methodology to the study of cellulose solvation by [C_4mim]Cl using the cellobiose model system. As detailed below, results from our MD simulations agree with previous theoretical and experimental studies, and, more importantly, corroborate the solvation model proposed by us in earlier reports.

2. Simulation Details

Classical MD simulations of neat [C_4mim]Cl and cellobiose/[C_4mim]Cl solutions were carried out using the CM3D package and the OPLS-AA force field modified as described in Section 3.1 (*6,7*). Partial charges were computed from fits to the electrostatic potential (ESP) derived from *ab initio* calculations at the B3LYP/6-311+G* level performed using Gaussian 03 (*8*). The geometries of an isolated [C_4mim]Cl pair and cellobiose, respectively, were optimized at the same level of theory prior to charge calculations. The optimized geometry of the single [C_4mim]Cl pair agrees well with results from *ab initio* MD simulations on [C_2mim]Cl (*9*), and shows that the chloride ion is localized above the plane of the imidazolium ring in close proximity to the C2 carbon. The charges computed for the cation and anion are +0.73 and -0.73, respectively. Following the approach employed in a reported MD study of [C_4mim]PF_6 (*10*), these partial charges were used to approximate the polarization of the ions in the liquid state in all our simulations. The disadvantage of this set of charges is that their

distribution on the atoms of the cation is based on its gas phase geometry, which is likely to differ from its structure in the liquid state. However, and as pointed out by Morrow and co-workers (*10*), this charge distribution gives no preferential orientation of the anions relative to the cations. Furthermore, the extent of polarization of the [C_4mim]Cl cation in the ion pair *in vacuo* relative to that of the isolated cation seen by us is similar to that observed for [C_4mim]PF_6 (*10*). Therefore, we tentatively conclude that the charges derived from *ab initio* calculations on the [C_4mim]Cl pair *in vacuo* are suitable for liquid phase simulations. While further tests will be conducted to verify this charge model, the results presented below validate these assumptions.

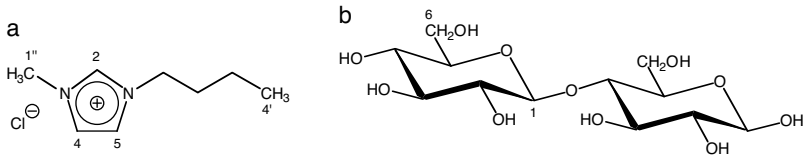

*Figure 1. Structure and numbering of [C_4mim]Cl (**a**) and cellobiose (**b**).*

The neat IL systems were simulated at seven temperatures, including 298, 313, 333, 343, 353, 363, and 373 K. The cellobiose/IL solution simulations were performed at 363 K with disaccharide concentrations of ~ 5 and ~ 10 wt%. These temperatures and sugar concentrations correspond to those from our previous NMR studies (*5*). Each system contained 216 ion pairs, totalling 5616 atoms. In addition, there were 6 and 12 cellobiose molecules for the 5 and 10 wt% cellobiose/IL systems, respectively. Periodic boundary conditions were employed, using the Ewald method to treat long-range electrostatic interactions (*11,12*). The reversible reference system propagator algorithm (r-RESPA) with time steps of 0.5 and 2 fs was employed to evaluate short-range intramolecular forces and long-range interactions, respectively (*13*). The neat [C_4mim]Cl system was constructed using the *ab initio* optimized ion pair as seed to create a cubic lattice with a final density of 1.0 g/cm^3. The system was then simulated at high temperature for at least 100 ps to randomize the ions in the cell. Constant temperature and pressure (NPT) simulations ranging from 100 ps to 1 ns were then carried out at each of the above temperatures and 1 atm to stabilize cell sizes. The cellobiose/IL model systems were created by patching the disaccharides on the sides of the equilibrated neat IL simulation box, and the resulting cells were randomized and their sizes stabilized as described above. The different systems were equilibrated at constant temperature (NVT) for times ranging from 700 ps to 1.5 ns. The neat IL systems were then simulated for an additional 2 ns at each temperature. For each cellobiose/IL system, 6 ns simulations were carried out. Coordinate files were saved every 0.1 ps in all cases, leading to 20,000 and 60,000 conformations used for the analysis of

structural and dynamic properties of the neat IL and cellobiose/IL systems, respectively. In addition, simulations for both cellobiose/IL systems were perfomed in duplicate from different initial configurations.

3. Neat [C_4mim]Cl Simulations

3.1. Optimization of Non-bonded Parameters

Our exploratory studies were carried out using default OPLS-AA parameters for the chloride ion (*6,14*). The density computed from NPT simulations at 298 K using these parameters was 0.80 g/cm^3, considerably lower than the value of 1.08 g/cm^3 determined experimentally at this temperature (*15*). We thus investigated the factors affecting the calculation of non-bonded interactions, which for two species *a* and *b* are represented by the sum of Coulomb and Lennard-Jones energy terms as shown in Equation 1 (*14*),

$$E_{ab} = \sum_{i}^{a}\sum_{j}^{b}\left\{\frac{q_i q_j e^2}{r_{ij}} + 4\varepsilon_{ij}\left[\left(\frac{\sigma_{ij}}{r_{ij}}\right)^{12} - \left(\frac{\sigma_{ij}}{r_{ij}}\right)^{6}\right]\right\} \quad (1)$$

where combining rules are used such that $\sigma_{ij} = (\sigma_{ii}\sigma_{jj})^{1/2}$ and $\varepsilon_{ij} = (\varepsilon_{ii}\varepsilon_{jj})^{1/2}$. Simulations starting from different initial configurations and various ion charge sets led only to minor changes on the density of the system. However, variations of the chloride ion Lennard-Jones parameters, σ and ε, had a pronounced effect on the computed densities. Not surprisingly, low densities were obtained by using default chloride ion OPLS-AA parameters (σ = 4.42 Å and ε = 0.12 kcal/mol), as these were optimized to fit interaction energies of ion-water complexes assuming an anion charge of -1.0. Based on our *ab initio* calculations, the partial charge for chloride in an ion pair has dropped to -0.73, indicating a reduction in the anion electron density and size. Similar reductions in size are likely for chloride ions in the IL, and thus Lennard-Jones parameters optimized for carbon-bound chlorine, σ = 3.40 Å and ε = 0.30 kcal/mol (*14*), could in principle be better suited to represent the free anion in molten [C_4mim]Cl. Indeed, repeating the NPT simulations at 298 K using these non-bonded parameters yields a density of 1.05 g/cm^3, which agrees well with the experimental density at this temperature. Figure 2 shows the simulated densities of neat [C_4mim]Cl as a function of temperature. As expected, the density decreases linearly with temperature, and volume expansions of less than 5% are observed as the system goes from 298 to 373 K (*10*).

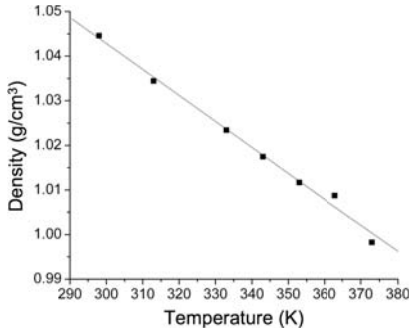

Figure 2. Density of neat [C_4mim]Cl as a function of temperature computed from MD simulations.

As described in the following sections, the structural and dynamic properties obtained from our MD simulations for neat [C_4mim]Cl agree well with experimental as well as classical and *ab initio* MD studies on similar systems. This has further validated our choice of force field and simulation conditions. The detailed analyses of the data summarized below are too vast to be presented here in full and will be made available elsewhere.

3.2. Structural Features of Neat [C_4mim]Cl

Figure 3 shows the cation-anion and cation-cation isotropic radial distribution functions (RDFs) computed from the center of mass of the imidazolium ring, $g_{ca}(r)$ and $g_{cc}(r)$, at the seven temperatures considered in our study. Their general characteristics agree well with those from previously reported MD simulations of ILs (*9,10,19-23*). Namely, $g_{ca}(r)$ and $g_{cc}(r)$ are out of phase, and also reveal that weak ordering due to long-range Coulombic interactions persists beyond 20 Å, which is approximately half of the unit cell and includes up to three coordination shells.

The first peak in the cation-anion RDF, located around 4.5 – 4.8 Å, represents the first coordination shell of chloride anions and is consisitent with results from experimental and theoretical studies (*16,19-23*). The coordination number is 3 when the RDF is integrated up to 5 Å, and 5 when integrated up to 6.5 Å, which corresponds to the first minimum of $g_{ca}(r)$. The sharpness of the peak indicates that the local structure is well defined, and coordination numbers of 3 to 5 point to the formation of ion clusters rather than pairs. This agrees with a structural model for *N*,*N*'-dialkylimidazolium salts based on an overview of experimental data proposed recently by Dupont (*17*). This author suggests that these ILs are hydrogen-bonded polymeric supramolecules, in which each cation

is surrounded by three anions that are approximately coplanar with the imidazolium ring and forming hydrogen bonds with its H2, H4, and H5 hydrogens. Similarly, each anion has three cations in its first coordination shell.

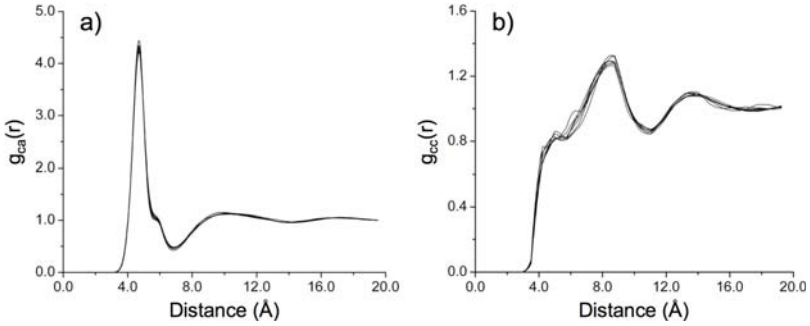

*Figure 3. Cation-anion (**a**) and cation-cation (**b**) RDFs for neat [C_4mim]Cl at temperatures ranging from 298 to 373 K.*

The cation-cation RDFs show a broad peak at 8 – 8.5 Å, and a clear shoulder, or 'bump,' around 4 – 6 Å with coordination numbers ranging from 1 to 2. A similar feature in the cation-cation RDF was detected experimentally and observed in theoretical studies for [C_2mim]Cl (*16,20,23*). While detailed 3D structural analyses of this salt in the liquid phase have not been reported, it has been postulated that these 'bumps' on $g_{cc}(r)$ are the result of π-π stacking interactions between imidazolium cations (*17*). Based on our analyses of the 3D distribution and angular distribution functions (ADFs) of cations (*vide infra*), we have indeed confirmed that the imidazolium rings π-π stack in [C_4mim]Cl.

As evidenced in Figure 3, the RDFs remain virtually unchangd as the system goes from 298 to 373 K. Similarly, there is only a minor decrease in the coordination numbers as the temperature increases, consistent with a slight decrease in the ordering of the system. This minimal increase in randomness agrees well with experimental findings which show that the ordering observed in crystals of *N*,*N*'-dialkylimidazolium salts is conserved in the liquid phase (*17*).

The RDFs provide short- and long-range structural features of the systems, but information regarding the spatial arrangement of ions is lost upon integration over angular space. To gain insights into the 3D structure of neat [C_4mim]Cl in the liquid phase, we computed 3D configuration probability distribution isosurfaces of ions relative to the center of a reference imidazolium ring. Figures 4a and 4b show, respectively, the chloride ion distribution isosurface drawn at 5 times the average anion density, and the imidazolium ion distribution isosurface drawn at 1.5 times the average cation density.

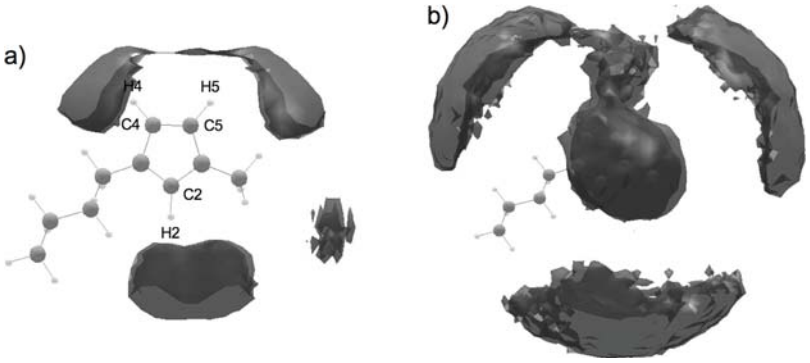

*Figure 4. 3D configuration probability distribution isosurfaces of [C_4mim]Cl anions (**a**) and cations (**b**) relative to the center of an imidazolium ring.*

In addition to 3D distribution isosurfaces such as the ones shown above, the ion ADFs with respect to a reference cation were analyzed in detail (data not shown). By combining the visual inspection of the distribution isosurfaces with quantitative analyses of RDFs and ADFs, the 3D structural features of [C_4mim]Cl can be summarized as follows. The ordering of the first coordination shells of an imidazolium cation is highly directional for anions and somewhat directional for cations. While the cation-anion and cation-cation RDFs indicate that weak ion ordering persists up to 20 Å, there is little preference in their angular distribution beyond the first coordination shells. The first anion coordination shell consists, on average, of five chloride ions, three of which are at less than 5 Å from the center of the ring and form hydrogen bonds with its H2, H4, and H5 hydrogens. These correspond with the three major lobes directed roughly along the C2-H2, C4-H4, and C5-H5 bonds observed in the anion distribution isosurface (Figure 4a). The probability of forming hydrogen bonds with H2 is significantly larger than with H4 and H5. The two additional anions in the first shell, located between 5 and 6.5 Å from the ring center, interact with the *N*-alkyl group hyrogens. The coordination number for the first shell of cations is 14.5. The majority of these cations coordinate to chloride ions in the first anion shell. Therefore, the cation distribution isosurface also shows three large lobes directed roughly along the C2-H2, C4-H4, and C5-H5 bonds, but at nearly twice the distance from the center of the ring than the first anion shell (Figure 4b). Finally, there are on average two cations whose rings lie parallel to that of the reference imidazolium ion located at only 4 to 6 Å from the ring center. These give rise to two lobes on the isosurface located above and below the ring, and reveal clearly that the imidazolium cations in [C_4mim]Cl are involved in π–π stacking interactions.

3.3. Dynamic Properties of Neat [C_4mim]Cl

The ability of our simulations to reproduce the dynamic behavior of the neat [C_4mim]Cl systems was assessed by comparing ion self-diffusion coefficients measured by PFG-NMR techniques to those computed from the MD trajectories using the Einstein relation (Equation 2):

$$D = \frac{1}{6}\lim_{t\to\infty}\frac{\left\langle\left|\Delta\mathbf{r}(t)^2\right|\right\rangle}{t} \tag{2}$$

$\langle|\Delta\mathbf{r}(t)^2|\rangle$ represents the average mean square displacements (MSDs) of the ions, which were calculated from the MD trajectories using the center of mass of the cation or anion (Figure 5). Cations and anions show similar diffusive behaviors and three distinct dynamic regimes. At very short times (< 0.1 ps) their motion is ballistic. Between 1 and 300 – 500 ps, the ions are sub-diffusive or 'caged,' with $\langle|\Delta\mathbf{r}(t)^2|\rangle \propto t^{\beta}$ ($\beta < 1$). After 500 ps, anions and cations display normal self-diffusivity, with $\langle|\Delta\mathbf{r}(t)^2|\rangle \propto t$. The dynamic behavior described here has been observed for other ILs studied by MD simulations (*10,19-21,24*). It is worth noting that the current study reveals that ions in [C_4mim]Cl are trapped in a super-cooled sub-diffusive regime for at least 100 ps even at temperatures nearly 40 K above its melting point.

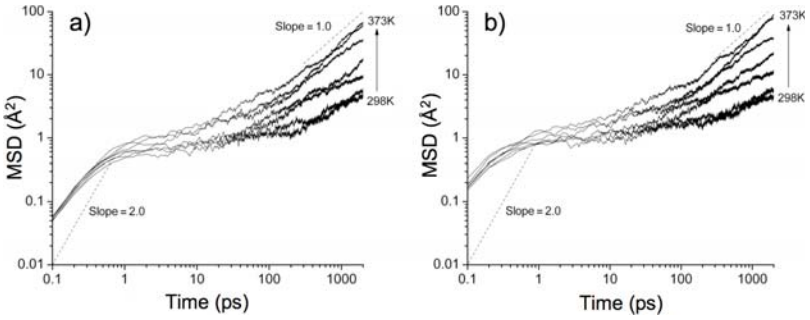

*Figure 5. Average MSDs for cations (**a**) and anions (**b**) versus time for neat [C_4mim]Cl at temperatures ranging from 298 to 373 K.*

Diffusion coefficients were estimated by fitting the linear self-diffusive regions of the MSDs to Equation 2 (*10,19,20*). Figure 6 shows a comparison of computed diffusion coefficients with those measured by NMR between 298 and 363 K. Below ~ 343 K (70 ^{o}C), our estimations for the imidazolium ion agree remarkably well with experiment. As expected, measured and computed

diffusion coefficients increase markedly after 343 K, slightly above the melting point of [C_4mim]Cl. While the computed values overestimate experiment above this temperature, the two sets of data remain in good semi-quantitative agreement. These results indicate that long-time quantities such as diffusion coefficients can be computed with reasonable accuracy in the simulation times considered in our study (*10*), and further validate our choice of force field parameters and simulation conditions for these systems.

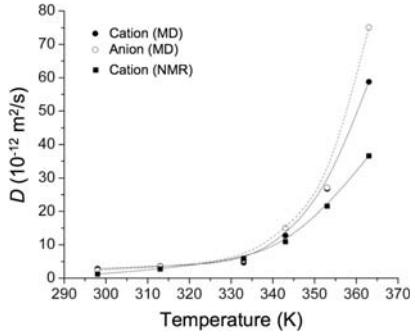

Figure 6. Computed and experimental diffusion coefficients for ions in neat [C_4mim]Cl as a function of temperature.

4. Cellobiose/[C_4mim]Cl Simulations

4.1 Solute-Solvent Interactions

The results presented in Section 3 indicate that our MD simulations are capable of reproducing structural and dynamic features of neat [C_4mim]Cl adequately, and we therefore turned our attention to the study of 5 and 10 wt% cellobiose/[C_4mim] solutions. As stated earlier, two independent 6 ns MD trajectories at 363 K were carried out for these systems. These parallel simulations led to virtually identical predictions, and therefore the analyses described here are based on results obtained for one of them.

The cellobiose-anion and cellobiose-cation center-of-mass RDFs show that the coordination shell closest to the disaccharide is within 4 – 6 Å of its center and contains mostly chloride ions. The first peak in the cellobiose-cation RDF is located at approximately 8 Å. This is in agreement with results from our recent

NMR studies, which reveal that anions have a more important role than cations in the dissolution of carbohydrates by this IL (*5*). However, the center-of-mass RDFs alone are ill-suited to describe the distribution of solvent ions around functional groups of the carbohydrate or specific solvent-solute interactions. Thus, we computed the RDFs from the hydroxyl protons to the chloride anions ($g_{OH\cdots Cl}(r)$, Figure 7a). Since the mobilities of the secondary and primary hydroxyl groups of the sugar are different, their $g_{OH\cdots Cl}(r)$ functions were considered separately. However, normalization over the number of equivalent hydroxyl groups yields RDFs that can be readily compared.

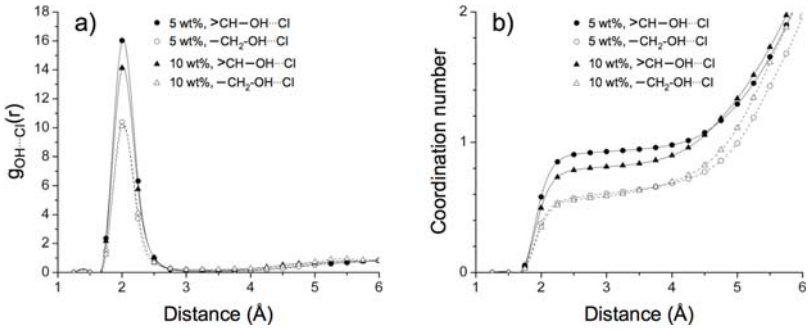

*Figure 7. OH···Cl RDFs (**a**) and coordination numbers (**b**) for 5 and 10 wt% cellobiose/[C_4mim]Cl solutions at 363 K.*

Irrespective of the type of hydroxyl group or sugar concentration, a single sharp peak at ~ 2 Å was observed in all $g_{OH\cdots Cl}(r)$ functions, strongly suggesting the formation of hydrogen bonds between the disaccharide hydroxyl protons and the chloride anions. Although their intensities are lower for primary hydroxyl groups, the position of the peaks is identical in all cases. Similarly, the coordination numbers of chloride ions to either primary or secondary hydroxyl protons plateaus at ~ 2.3 Å and remains almost constant up to ~ 4 Å (Figure 7b). Beyond that distance, the coordination numbers increases due to interactions between ions in the first anion shell and protons in neighboring hydroxyl groups. For the 5 wt% cellobiose/[C_4mim]Cl solution, the coordination numbers of secondary and primary hydroxyl groups to chloride ions in the first shell are 0.93 and 0.60, respectively. In the 10 wt% solution these values are 0.82 and 0.59, consistent with the decrease in anion supplies at higher carbohydrate concentrations. The variations in coordination numbers observed for the different types of hydroxyl groups indicate that the chloride ions have a higher probability of forming hydrogen bonds with secondary hydroxyl protons. Additionally, the anion to primary hydroxyl proton coordination numbers remain nearly constant at both sugar concentrations, revealing that the average

number of hydrogen bonds between these two species is not affected by changes in the supplies of chloride ions.

The geometry of the hydrogen bonds formed between hydroxyl protons and anions was investigated by analysis of the probability distribution of O–H···Cl angles. Since the OH···Cl coordination numbers are less than 1 in all cases, the O–H···Cl angles were calculated using the chloride ions located closest to the hydroxyl protons. As shown in Figure 8, almost all O–H···Cl angles are within 150 and 180°, and thus in near-perfect hydrogen-bonding geometry. Combined with the analysis of OH···Cl RDFs presented above, these results confirm conclusively that medium to strong hydrogen bonds form between the sugar hydroxyl protons and the chloride ions of the IL.

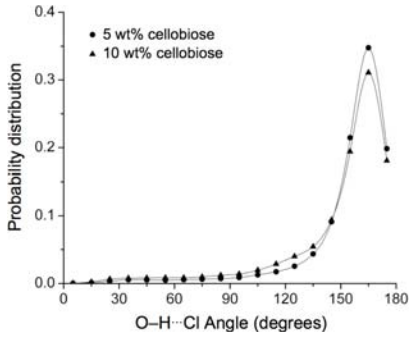

Figure 8. Probability distribution of O–H···Cl angles in 5 and 10 wt% cellobiose/[C_4mim]Cl solutions at 363 K

Averaging the anion to hydroxyl proton coordination numbers over all types of hydroxyl groups yields OH···Cl hydrogen-bonding stoichiometries of 1:0.85 and 1:0.76 for the 5 and 10 wt% cellobiose/[C_4mim]Cl solutions, respectively. These values depart slightly from the ideal 1:1 ratio expected for these systems. Analysis of several saved conformations from the MD trajectories indicates that this is due to the occasional formation of intra- or inter-molecular hydrogen bonds between sugar hydroxyl protons and oxygen atoms on other hydroxyl or ether groups. Both types of hydroxyl groups can do this, but the added flexibility of the hydroxymethyl side chains allows for more intra-molecular hydrogen-bonding interactions, and thus lower coordination numbers for these groups.

As shown in the next sections, the cellobiose/IL systems have slower dynamics than the neat IL systems. Thus, the minor deviations in our predicted OH···Cl hydrogen-bonding stoichiometries from the theoretical 1:1 ratio could be due to insufficient sampling times. However, it should also be noted that this ideal OH:Cl ratio can only be achieved in solutions with a large execss of chloride ions (i.e., infinite dilution), which is not the case in these systems.

Despite this, our predictions are in excellent agreement with results from earlier NMR relaxation measurements on the cellobiose/[C_4mim]Cl system, which also indicate that OH···Cl interactions are nearly stoichiometric (*5*). Combined, our previous experimental findings and those presented here demonstrate conclusively that hydrogen-bonding interactions between non-hydrated chloride ions and sugar hydroxyl protons play a key role in the dissolution of carbohydrates in [C_4mim]Cl.

4.2. Solvent Structuring in Cellobiose/[C_4mim]Cl Solutions

The effects on the structuring of [C_4mim]Cl due to the precense of sugar solutes was also investigated. The overall structural features of the solvent are very similar to those of the neat ILs in terms of positions of the first anion and cation coordination shells, coordination numbers, angular distributions, and hydrogen-bonding patterns between anions and imidazolium ring protons. Anion-cation and cation-cation coordination numbers decrease slightly relative to neat [C_4mim]Cl, which is reasonable if the solute-solvent interactions described in the previous section are taken into account.

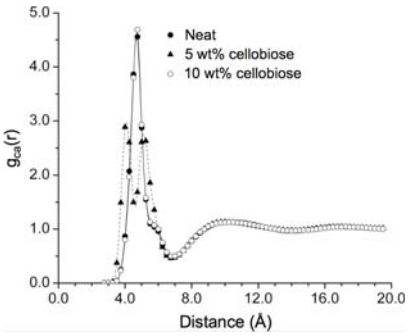

Figure 9. Cation-anion RDFs for neat [C_4mim]Cl and cellobiose/[C_4mim]Cl solutions at 363 K.

Although the overall solvent structuring in the systems is similar, the cation-anion RDF for the 5 wt% cellobiose/[C_4mim]Cl solution exhibits a feature that distinguishes it from the neat IL and 10 wt% cellobiose/IL systems. As shown in Figure 9, the first peak of cation-anion RDF in this system is split in two. Detailed analysis of the MD trajectories shows that this is caused by an uneven distribution of disaccharides in the simulation box that leads to a cellobiose-rich region and one in which no sugars are present. By increasing the number of solutes in the unit cell from 6 (5 wt%) to 12 (10 wt%) their

distribution becomes uniform, leading to a unique peak in the RDF. While these results could reflect the formation of solute clusters at lower sugar concentrations, they are more likely artifacts caused by inadequate equilibration and/or conformational sampling of the systems. Additional simulations are currently being carried out to address these issues.

4.3. Dynamic Properties of Cellobiose/[C_4mim]Cl Solutions

The MSDs of the cellobiose/[C_4mim]Cl solutions at 363 K are very similar to those presented in Section 3.3 for the neat [C_4mim]Cl systems, and display ballistic, sub-diffusive, and normal self-diffusive regimes. The cation, anion, and cellobiose self-diffusion coefficients were computed by fitting the linear regions of the MSDs in the normal diffusive regime to Equation 2 as described above. As mentioned earlier, two independent simulations for both cellobiose/[C_4mim]Cl solutions were carried out. Since their differences are negligible, the diffusivities presented here are averages from both MD trajectories recorded for each system. Not surpisingly, the dynamics of the cellobiose/IL solutions are considerably slower than for the neat [C_4mim]Cl systems. The diffusion coefficient for the cation drops from 58.8×10^{-12} m^2/s for the neat IL to 19.8×10^{-12} and 10.4×10^{-12} m^2/s at 5 and 10 wt% cellobiose, respectively. Similarly, the anion diffusion coefficient decreases from 75.1×10^{-12} in the neat IL to 21.9×10^{-12} m^2/s at 5 wt% cellobiose, and to 13.2×10^{-12} m^2/s at 10 wt% cellobiose. Consistent with its size, the self-diffusivities computed for the disaccharide are 4.1×10^{-12} and 2.6×10^{-12} m^2/s at 5 and 10 wt% concentration, respectively. These results agree qualitatively with reported variations in the viscosity of cellobiose/[C_4mim]Cl solutions versus sugar concentration (*5*), as well as with cation diffusion coefficients measured for these systems using PFG-NMR methods. However, the changes in diffusivities predicted from the MD simulations are nearly three-fold larger than those determined experimentally. As stated in the previous sections and discussed below, we believe that these deviations are due to improper and/or insufficient sampling of the conformational space available to the systems.

5. Conclusions

In this paper, MD simulations of neat [C_4mim]Cl at various temperatures and of cellobiose/[C_4mim]Cl solutions were performed in an attempt to better understand how this IL dissolves carbohydrates at the molecular level. The calculated properties of the neat IL derived from our simulations agree well with those from previously reported experimental and theoretical studies on similar systems. Structural analysis shows long-range ordering of ions as well as

directional ordering of the first anion and cation coordination shells. Anions in the first shell form hydrogen bonds with the ring hydrogen atoms and also interact with hydrogens in the alkyl chains. Most of the first cation shell is located well outside the first shell of anions, but a small portion of it stays above and below the ring, revealing that the imidazolium cations in [C_4mim]Cl participate in π-π stacking interactions. The calculated self-diffusion coefficients at various temperatures agree semi-quantitatively with results from PFG-NMR measurements, indicating that the dynamic properties of the neat IL are described with reasonable accuracy by the MD simulations.

MD simulations of cellobiose/[C_4mim]Cl solutions reveal the formation of medium to strong hydrogen bonds between the disaccharide hydroxyl protons and the IL chloride ions in a near 1:1 ratio, in excellent agreement with results from previous NMR studies. More importantly, our findings demonstrate clearly that these hydrogen-bonding interactions are responsible for the high solubility observed for many carbohydrates and polysaccharides in this IL. While a recent report speculates that interactions between the imidazolium cations and the sugar hydroxyl oxygens play a critical role in the dissolution process (*25*), our experimental and theoretical studies provide no evidence in support of these claims. On the contrary, they show that the cations are far from the solute and interact solely with chloride ions in the first solvation shell of the sugar.

The results presented here also indicate that while our current simulations reproduce trends in the dynamics of the cellobiose/[C_4mim]Cl systems, they cannot yet predict these properties quantitatively. Although MD simulations of similar lengths have been used successfully to investigate dynamic properties of IL solutions (*26,27*), the solutes considered in these studies were small weakly-coordinating molecules such as acetonitrile or CO_2. In our case, the solvated molecule is significantly larger, flexible, and interacts strongly with the solvent, and as a result the dynamics of the systems are considerably slower. Thus, the sugar/IL solutions are likely to require more extensive system equilibration and conformational sampling times to yield accurate atomistic dynamic models. Work on the improvement of these aspects of our simulations is underway. Ultimately, the information gathered from our ongoing experimental and theoretical studies should facilitate the rational development of new, and potentially 'greener,' IL-based solvent systems for the dissolution and processing of polysaccharides with industrial applications.

Ackonwledgment. The authors acknowledge the H. O. West Foundation, the NSF CCLI-A&I and MRI programs (grants DUE-9952264 and CHE-0420556), and the Camille and Henry Dreyfus Foundation for financial support. We also thank Dr. Gonzalo Hernandez for performing the PFG-NMR measurements of cation diffusivities in neat [C_4mim]Cl and cellobiose/[C_4mim]Cl solutions.

References

1) *Ionic Liquids IIIA/B: Fundamentals, Progress, Challenges, and Opportunities*; Rogers, R. D., Seddon, K. R., Eds.; ACS Symposium Series 901/902; American Chemical Society: Washington, DC, 2005.
2) Swatloski, R. P.; Spear, S. K.; Holbrey, J. D.; Rogers, R. D. *J. Am. Chem. Soc*. **2002**, *124*, 4974-4975.
3) Liu, Q. B.; Janssen, M. H. A.; van Rantwijk, F.; Sheldon, R. A. *Green Chem*. **2005**, *7*, 39-42.
4) Fort, D. A.; Swatloski, R. P.; Moyna, P.; Rogers, R. D.; Moyna, G. *Chem. Commun*. **2006**, 716-718.
5) Remsing, R. C.; Swatloski, R. P.; Rogers, R. D.; Moyna, G. *Chem. Commun*. **2006**, 1271-1273.
6) http://hydrogen.usip.edu/moore/code/code.html.
7) Jorgensen, W. L.; Maxwell, D. S.; Tirado-Rives, J. *J. Am. Chem. Soc.* **1996**, *118*, 11225-11236.
8) Frisch, M. J.; Trucks, G. W.; Schlegel, H. B.; Scuseria, G. E.; Robb, M. A.; Cheeseman, J. R.; Montgomery, Jr., J. A.; Vreven, T.; Kudin, K. N.; Burant, J. C.; Millam, J. M.; Iyengar, S. S.; Tomasi, J.; Barone, V.; Mennucci, B.; Cossi, M.; Scalmani, G.; Rega, N.; Petersson, G. A.; Nakatsuji, H.; Hada, M.; Ehara, M.; Toyota, K.; Fukuda, R.; Hasegawa, J.; Ishida, M.; Nakajima, T.; Honda, Y.; Kitao, O.; Nakai, H.; Klene, M.; Li, X.; Knox, J. E.; Hratchian, H. P.; Cross, J. B.; Bakken, V.; Adamo, C.; Jaramillo, J.; Gomperts, R.; Stratmann, R. E.; Yazyev, O.; Austin, A. J.; Cammi, R.; Pomelli, C.; Ochterski, J. W.; Ayala, P. Y.; Morokuma, K.; Voth, G. A.; Salvador, P.; Dannenberg, J. J.; Zakrzewski, V. G.; Dapprich, S.; Daniels, A. D.; Strain, M. C.; Farkas, O.; Malick, D. K.; Rabuck, A. D.; Raghavachari, K.; Foresman, J. B.; Ortiz, J. V.; Cui, Q.; Baboul, A. G.; Clifford, S.; Cioslowski, J.; Stefanov, B. B.; Liu, G.; Liashenko, A.; Piskorz, P.; Komaromi, I.; Martin, R. L.; Fox, D. J.; Keith, T.; Al-Laham, M. A.; Peng, C. Y.; Nanayakkara, A.; Challacombe, M.; Gill, P. M. W.; Johnson, B.; Chen, W.; Wong, M. W.; Gonzalez, C.; Pople, J. A. *Gaussian 03*; Gaussian, Inc.: Wallingford, CT, 2004.
9) Del Pópolo, M. G.; Lynden-Bell, R. M.; Kohanoff, J. *J. Phys. Chem. B* **2005**, *109*, 5895-5902.
10) Morrow, T. I.; Maginn, E. J. *J. Phys. Chem. B* **2002**, *106*, 12807-12813; **2003**, *107,* 9160.
11) Darden, T. A.; York, D. M.; Pedersen, L. G. *J. Chem. Phys.* **1993,** *98,* 10089-10092.
12) Essmann, U.; Perera, L.; Berkowitz, M. L.; Darden, T.; Lee, H.; Pedersen, L. G. *J. Chem. Phys*. **1995,** *103,* 8577-8593.
13) Tuckerman, M.; Berne, B.; Martyna, G. *J. Chem. Phys.* **1992**, *97*, 1990-2001.

14) Chandrasekhar, J.; Spellmeyer, D. C.; Jorgensen, W. L. *J. Am. Chem. Soc.* **1984,** *106,* 903-910.
15) Huddleston, J. G.; Visser, A. E.; Reichert, W. M.; Willauer, H. D.; Broker, G. A.; Rogers, R. D. *Green Chemistry,* **2001,** *3*, 156-164.
16) Hardacre, C.; Holbery, J. D.; McMath, S. E. J.; Bowron, D. T.; Soper, A. K. *J. Chem. Phys.* **2003**, *118,* 273-278.
17) Dupont, J. *J. Braz. Chem. Soc.* **2004,** *15,* 341-350.
18) Hanke, C. G.; Price, S. L.; Lynden-Bell, R. M. *Mol. Phys.* **2001,** *99,* 801-809.
19) Margulis, C. J.; Stern, H. A.; Berne, B. J. *J. Phys. Chem. B* **2002,** *106,* 12017-12021.
20) Yan, T.; Burnham, C. J.; Del Pópolo, M. G.; Voth, G. A. *J. Phys. Chem. B* **2004,** *108,* 11877-11881.
21) Del Pópolo, M. G.; Voth, G. A. *J. Phys. Chem. B.* **2004,** *108,* 1744-1752.
22) Bühl, M.; Chaumont, A.; Schurhammer, R.; Wipff, G. *J. Phys. Chem. B.* **2005,** *109,* 18591-18599.
23) Bhargava, B. L.; Balasubramanian, S. *Chem. Phys. Lett.* **2006,** *417,* 486-491.
24) Hu, Z.; Margulis, C. J. *Proc. Natl. Acad. Sci.* **2006,** *103,* 831-836.
25) Zhang, H.; Wu, J.; Zhang, J.; He, J. *Macromolecules*, **2005**, *38*, 8272-8277.
26) Wu, X.; Liu, Z.; Huang, S.; Wang, W.; *Phys. Chem. Chem. Phys.* **2005,** *7,* 2771-2779.
27) Huang, X.; Margulis, C. J.; Li, Y.; Berne, B. J. *J. Am. Chem. Soc.* **2005,** *127,* 17842-17851.